Instability of charged Lovelock black holes: Vector perturbations and scalar perturbations

AUTHOR(S):

Takahashi, Tomohiro

CITATION:

Takahashi, Tomohiro. Instability of charged Lovelock black holes: Vector perturbations and scalar perturbations. Progress of Theoretical and Experimental Physics 2013, 2013(1): 13E02.

ISSUE DATE:

2013-01

URL:

http://hdl.handle.net/2433/173805

PTEP
Prog. Theor. Exp. Phys. **2013**, 013E02 (25 pages)
DOI: 10.1093/ptep/pts049

Instability of charged Lovelock black holes: Vector perturbations and scalar perturbations

Tomohiro Takahashi[1]*

[1]*Department of Physics, Kyoto University, Kyoto, 606-8502, Japan*
*E-mail: takahashi@tap.scphys.kyoto-u.ac.jp

Received September 22, 2012; Revised October 15, 2012; Accepted October 17, 2012; Published January 1, 2013

We examine the stability of charged Lovelock black hole solutions under vector-type and scalar-type perturbations. We find suitable master variables for the stability analysis; the equations for these variables are Schrödinger-type equations with two components, and these Schrödinger operators are symmetric. By these master equations, we show that charged Lovelock black holes are stable under vector-type perturbations. For scalar-type perturbations, we show the criteria for instability and check these numerically. In our previous paper [T. Takahashi, Prog. Theor. Phys. **125**, 1289 (2011)], we have shown that nearly extreme black holes show instability under tensor-type perturbations. In this paper, we find that black holes with a small charge show instability under scalar-type perturbations even if they have a relatively large mass.

Subject Index E03, E04

1. Introduction

The braneworld scenario with large extra dimensions predicts that higher dimensional black holes might be produced at colliders [1,2]. Therefore, higher dimensional black holes become attracting subjects and some aspects of these have been inspected so far. For example, exact solutions are investigated in higher dimensions. In higher dimensions, besides Schwarzschild black holes, Reissner–Nordström black holes [3], and rotating black holes [4], various solutions are found: the black ring solution [5], the black di-ring [6], the black Saturn [7] and so on. From the standpoint of black hole creation, it is important to examine the stability of such solutions because stationary solutions with instabilities are not attractors of time evolutions. This suggests that such black holes should not be realized.

So far, various stability analyses for black hole solutions have been performed. One of the most notable analyses is that of Tangherlini–Schwarzschild solutions by Kodama and Ishibashi [8–10]. They have derived master equations for all types of perturbations. These are Schrödinger-type equations and they have shown that these Schrödinger operators are all positive-definite using the S-deformation approach that they have developed by Friedrichs extension. These results show that Schwarzschild black holes are also stable in higher dimensions. They have also examined the stability of higher dimensional Reissner–Nordström black holes [11]. By the S-deformation, they have also shown that this charged solution is stable under tensor- and vector-type perturbations. For scalar-type perturbations, it has been shown that this black hole is stable in 4 and 5 dimensions. For this solution, the stability has also been studied numerically and it has been found that black holes with large

negative cosmological constants and large charge are unstable in more than 7 dimensions [12]. On Myers–Perry black hole solutions, in $D \geq 6$, there exists the instability for singly rotating solutions when the spin parameter is large enough [13–15]. In even dimensions, the stability of the near-horizon geometry of rotating black holes with equal angular momenta is investigated [16]. It has been suggested that scalar modes for the base space show instability. Recently, the stability of the black ring solution has been examined by using the local Penrose inequality and it has been shown that the fat branch is unstable [17].

The stability analyses we have introduced above are all premised on Einstein theory. In fact, the stability of black hole solutions has mainly been examined in Einstein theory. This is as important as such analyses to investigate the stability in more general theories. In 4 dimensions, Einstein theory is characterized by two properties: the action has the general coordinate covariance and the equation of motion consists of the metric, the first derivative of the metric, and the second derivative of the metric [18]. Then it is natural to extend the 4-dimensional gravitational theory to a higher dimensional one keeping these two properties. In higher dimensions, the most general theory that satisfies the above two features is not Einstein theory; it is Lovelock theory [19]. Thus it is important to generalize the stability analyses of black hole solutions in Einstein theory to those in Lovelock theory.

In Lovelock theory, a spherically symmetric black hole solution is known. This was first found in second-order Lovelock theory [20,21] and extended to general Lovelock theory [22–26]. For this so-called Lovelock black hole solution, the stability has been analyzed in Refs. [27–33]. In these papers, it has been shown that black holes with sufficiently small mass are unstable under scalar-type perturbations in odd dimensions and unstable under tensor-type perturbations in even dimensions. This critical mass differs with dimension and Lovelock coupling. These instabilities become stronger as the wavelength becomes smaller, and the time scale of the instability converges to 0 in the small-scale limit. Under vector perturbations, this solution is stable in all dimensions; this is independent of the mass.

Since black hole creations originate from protons at colliders, it is also important to take account of Maxwell charge. In Lovelock theory with the $U(1)$ field, a charged black hole solution is known [22–25]; this has spherical symmetry and a time-like Killing vector, and this Reissner–Nordström like solution is called the charged Lovelock black hole solution. Thus, in this paper, we would like to extend the stability analysis for Lovelock black hole solutions to charged Lovelock black hole solutions. For this charged solution, the stability analysis under tensor-type perturbations has been examined by us and we have shown that black holes are unstable if they have nearly extreme mass [34]. In this paper, we extend our previous discussion to vector-type perturbations and scalar-type perturbations; i.e., we derive master equations for these types of perturbations and examine the stability using these master equations.

The organization of this paper is as follows. In Sect. 2, we review Lovelock theory, present the charged Lovelock black hole solutions, and check the behaviors of these solutions. We mainly concentrate on the asymptotically flat branch. In Sect. 3, we review the analysis for tensor-type perturbations [34]. We examine tensor perturbations and show the criteria for stability under these perturbations. In Sect. 4, we derive master equations for vector-type perturbations and show that there is no instability under this type of perturbation. In Sect. 5, we concentrate on scalar-type perturbations. We show that the master equations can be summarized as a Schrödinger-type equation with two components, and using this equation we present criteria for stability. In Sect. 6, we numerically examine the conditions for instability presented in Sects. 3 and 5. In this paper, we only check in 5–8 dimensions. In the final section, Sect. 7, we summarize this paper.

2. Charged Lovelock black holes

In this section, we introduce Lovelock theory and present charged black hole solutions in Lovelock–Maxwell theory. These solutions are expressed as the roots of the polynomial equation and we confirm that one of the roots is asymptotically flat. For this asymptotically flat root, we briefly check the behavior, the singularity, and the horizon.

2.1. *Lovelock–Maxwell system*

In Ref. [19], D. Lovelock constructed the gravitational theory, the equation of motion of which consists of the metric, the first derivative of the metric, and the second derivative of the metric. The Lagrangian for this theory is

$$\mathcal{L}_{\text{Lovelock}} = -2\Lambda + \beta_1 R + \sum_{m=2}^{k} \frac{\beta_m (2m)!}{2^m m \prod_{p=1}^{2m-2}(n-p)} \delta^{[\lambda_1}_{\kappa_1}\delta^{\sigma_1}_{\rho_1}\delta^{\lambda_2}_{\kappa_2}\cdots\delta^{\sigma_m]}_{\rho_m} R_{\lambda_1\sigma_1}{}^{\kappa_1\rho_1}\cdots R_{\lambda_m\sigma_m}{}^{\kappa_m\rho_m},$$

where Λ corresponds to a cosmological constant and β_ms are arbitrary constants that we call Lovelock couplings. We add the coefficients $(2m)!/2^m m\prod_{p=1}^{2m-2}(n-p)$ for convenience. In the above Lagrangian, n is related to the dimension D as $n = D-2$ and k corresponds to the maximum order defined as $k \equiv [(D-1)/2]$ where $[x]$ is the Gauss symbol. There exists a maximum order k due to the antisymmetric property of $\delta^{[\lambda_1}_{\kappa_1}\delta^{\sigma_1}_{\rho_1}\delta^{\lambda_2}_{\kappa_2}\cdots\delta^{\sigma_m]}_{\rho_m}$. When we fix the maximum order k, the dimension is restricted as $n = D-2 = 2k-1, 2k$; e.g., the second-order Lovelock theory is the most general in $n = 3$ or $n = 4$, and the third-order one is in $n = 5$ or $n = 6$. By the ambiguity of the overall factor of the action, we take the unit $\beta_1 = 1$ in this paper.

In this paper, we want to concentrate on the Lovelock–Maxwell system. This system is described by the action

$$S = \int d^D x\sqrt{-g}\mathcal{L}_{\text{Lovelock}} - \int d^D x\sqrt{-g}\frac{1}{4}F_{\mu\nu}F^{\mu\nu}, \tag{1}$$

where $F_{\mu\nu}$ is the field strength of Maxwell field A_μ. In action (1), the dynamical variables are $g_{\mu\nu}$ and A_μ. Variations of these variables lead to

$$\mathcal{G}_\mu{}^\nu = T_\mu{}^\nu, \tag{2}$$

$$F^{\mu\nu}{}_{;\nu} = 0, \tag{3}$$

where $\mathcal{G}_\mu{}^\nu$, which we call the Lovelock tensor, and $T_\mu{}^\nu$, which is the energy momentum tensor for the $U(1)$ field, are defined as

$$\mathcal{G}_\mu{}^\nu = \Lambda\delta^\nu_\mu + R_\mu{}^\nu - \frac{1}{2}R\delta_\mu{}^\nu - \sum_{m=2}^{k}\frac{(2m+1)!}{2^{m+1}}\frac{\beta_m}{m\prod_{p=1}^{2m-2}(n-p)}\delta^{[\nu}_{\mu}\delta^{\lambda_1}_{\kappa_1}\delta^{\sigma_1}_{\rho_1}\delta^{\lambda_2}_{\kappa_2}\cdots\delta^{\sigma_m]}_{\rho_m}R_{\lambda_1\sigma_1}{}^{\kappa_1\rho_1}\cdots R_{\lambda_m\sigma_m}{}^{\kappa_m\rho_m}, \tag{4}$$

$$T_\mu{}^\nu = F_{\mu\lambda}F^{\nu\lambda} - \frac{1}{4}F_{\lambda\rho}F^{\lambda\rho}\delta^\nu_\mu. \tag{5}$$

The field strength is defined as $F = dA$, thus $F_{\mu\nu}$ must satisfy the identity

$$dF = 0 \Rightarrow F_{[\mu\nu;\lambda]} = 0. \tag{6}$$

The above equations (2), (3), and (6) are our basic equations.

2.2. *Charged Lovelock black holes*

For the basic equations, black hole solutions with two parameters are known [22–25]. We assume a static spherically symmetric metric with a spherically symmetric electric field

$$ds^2 = -f(r)dt^2 + 1/f(r)dr^2 + r^2\gamma_{ij}dx^i dx^j, \tag{7}$$

$$F^{tr} = E(r), \quad \text{other components} = 0. \tag{8}$$

In these, γ_{ij} corresponds to the metric for S^n.

We can easily check that these ansätze satisfy (6). Thus we concentrate on the others and these lead to the following equations:

$$\begin{aligned} F^{t\mu}{}_{;\mu} = 0 &\Rightarrow \partial_r(r^n E(r)) = 0, \\ \mathcal{G}_i{}^j = T_i{}^j &\Rightarrow -\frac{1}{2r^{n-1}}\left(r^{n+1}\mathcal{P}[\psi]\right)'' \delta_i^j = \frac{E^2}{2}\delta_i^j, \\ \mathcal{G}_t{}^t = T_t{}^t,\ \mathcal{G}_r{}^r = T_r{}^r &\Rightarrow -\frac{n}{2r^n}\left(r^{n+1}\mathcal{P}[\psi]\right)' = -\frac{E^2}{2}, \end{aligned} \tag{9}$$

and the other components are identical. In (9), ψ is related to $f(r)$ as $f = 1 - r^2\psi$ and $\mathcal{P}[\psi]$ is defined as

$$\mathcal{P}[\psi] \equiv \sum_{m=2}^{k}\left[\frac{\beta_m}{m}\psi^m\right] + \psi - \frac{2\Lambda}{n(n+1)}. \tag{10}$$

The second equation of (9) is derived by a derivative of the third equation with the first equation, so we only consider the first and third equations. The first equation can be easily integrated and the result is

$$E(r) = \sqrt{n(n-1)}\mathcal{Q}/r^n. \tag{11}$$

In this equation, $\sqrt{n(n-1)}\mathcal{Q}$ is an integral constant and this constant corresponds to the charge, which can be seen from the behavior of $E(r)$. Substituting (11) into the third equation of (9), we can gain $\left(r^{n+1}\mathcal{P}[\psi]\right)' = (n-1)\mathcal{Q}^2/r^n$, or integrating both sides reads

$$\mathcal{P}[\psi] = \frac{\mathcal{M}}{r^{n+1}} - \frac{\mathcal{Q}^2}{r^{2n}} \equiv M(r), \tag{12}$$

where $\mathcal{M}$ is an integral constant. We will see that $\mathcal{M}$ corresponds to the mass when checking the asymptotic behavior of the solution [35,36].

We must solve the polynomial equation (12) for solutions of the Lovelock–Maxwell system. In order to solve the polynomial equation (12), in this paper, we assume some conditions for the Lovelock couplings β_m and $\mathcal{M}$ for simplicity. First, we consider that the mass of the black hole is positive, i.e., $\mathcal{M} > 0$. Second, we set the cosmological constant $\Lambda = 0$. For $\Lambda = 0$, as we will see later, there must exist an asymptotically flat branch. Third, for simplicity, we assume the positivity of the Lovelock couplings, i.e.,

$$\beta_m > 0 \ (m \geq 2). \tag{13}$$

2.3. *Asymptotically flat branch*

Because (12) is the kth-order polynomial, the polynomial equation (12) should have at most k solutions. However, assuming all Lovelock couplings are positive and $\Lambda = 0$, one of the roots corresponds to an asymptotically flat solution.

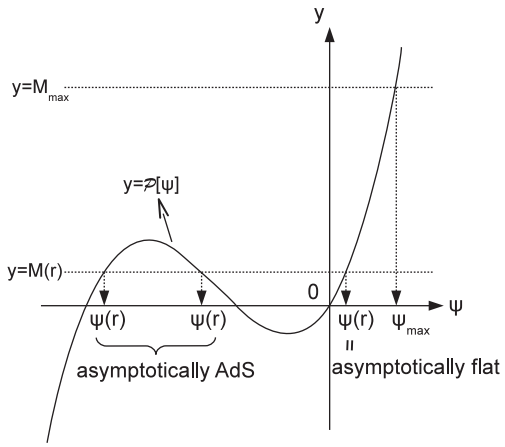

Fig. 1. We introduce the graphical method for finding the roots of (12) in this figure. The solid curve corresponds to $y = \mathcal{P}[\psi]$ and the dotted horizontal line is $y = M(r)$ with fixed r. The cross points in this figure are the solutions of the polynomial equation (12) for this r. If we want to consider the roots for other radii, we draw the corresponding dotted line $y = M(r)$ and see the cross points.

For instance, we see the above statement when $k = 2$. In this case, (12) reduces into the second-order polynomial equation, so this can be easily solved as

$$\psi(r) = \begin{cases} (-1 + \sqrt{1 + 2\beta_2 \mathcal{M}/r^{n+1} - 2\beta_2 \mathcal{Q}^2/r^{2n}})/\beta_2 \\ (-1 - \sqrt{1 + 2\beta_2 \mathcal{M}/r^{n+1} - 2\beta_2 \mathcal{Q}^2/r^{2n}})/\beta_2 \end{cases} . \tag{14}$$

Let us consider the limit $r \to \infty$. The first root behaves as $\psi \to \mathcal{M}/r^{n+1}$ and the second converges as $\psi \to -2/\beta_2$. Therefore, the function $f(r) = 1 - r^2\psi(r)$ behaves as $f = 1 - \mathcal{M}/r^{n-1}$ for the first root and $f = 1 + 2r^2/\beta_2$ for the second one. This shows that the first branch expresses an asymptotically flat solution and the other is an asymptotically AdS solution.

Regrettably, we cannot write the roots of Eq. (12) with general k explicitly. Nevertheless, we can understand the existence of an asymptotically flat solution as the solution of (12). In order to check this statement, we want to introduce the graphical method. In Fig. 1, we show $y = M(r)$ with fixed r and $y = \mathcal{P}[\psi]$ in the $\psi - y$ diagram. The former is a horizontal line because M depends only on r and we fix r. The cross points in Fig. 1 are the roots of the polynomial equation (12) for this fixed r, and if we want to find the roots for other radii, we move the horizontal line following the value of $M(r)$ and check the cross points.

For this method, it is important to check the behavior of $M(r) = \mathcal{M}/r^{n+1} - \mathcal{Q}^2/r^{2n}$. Its first derivative is $M'(r) = -\frac{(n+1)\mathcal{M}}{r^{2n+1}}\left(r^{n-1} - \frac{2n\mathcal{Q}^2}{(n+1)\mathcal{M}}\right)$. Then, like Fig. 2, $M(r)$ becomes 0 at $r = r_0 = \left(\mathcal{Q}^2/\mathcal{M}\right)^{\frac{1}{n-1}}$, takes the maximum value $M_{\max} = \frac{n-1}{2n}\mathcal{M}\left(\frac{(n+1)\mathcal{M}}{2n\mathcal{Q}^2}\right)^{\frac{(n+1)}{(n-1)}}$ at $r = r_{\max=}$ $(2n/(n+1))^{\frac{1}{n-1}} r_0$, and behaves as $M \sim \mathcal{M}/r^{n+1}$ in the asymptotic region.

As mentioned above, $M(r)$ is positive in $r > r_0$. While $M(r)$ is positive, from Fig. 1, the polynomial equation (12) has only one positive root because $\mathcal{P}[\psi]$ satisfies $\mathcal{P}[0] = 0$ and is a monotonically increasing function in $\psi > 0$ under our assumptions (13). This positive root expresses an asymptotically flat solution. To confirm this, let us consider the behavior of this ψ when $r \to \infty$. Because $M(r)$ converges to 0 like $\mathcal{M}/r^{n+1}$ as $r \to \infty$, the positive cross point in Fig. 1 also converges to 0. In detail, Eq. (12) with $\psi \sim 0$ shows that this root converges like $\psi \sim \mathcal{M}/r^{n+1}$. Then, for this branch, $f(r)$ behaves as $f(r) \sim 1 - \mathcal{M}/r^{n-1}$ in the asymptotic region. The metric ansatz (7) with

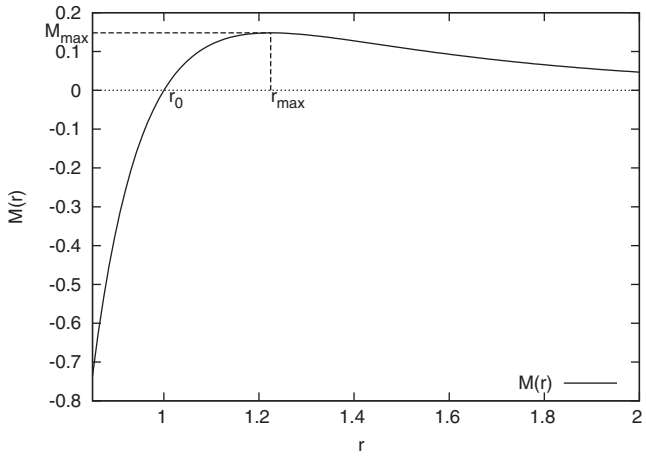

Fig. 2. We plot $M(r)$ with $n = 3$, $\mathcal{M} = 1$, and $\mathcal{Q} = 1$ in this figure. r_0 and $r_{\max}$ is defined as $M(r_0) = 0$ and $M'(r_{\max}) = 0$ respectively. $M_{\max}$ corresponds to $M(r_{\max})$. We can recognize the manners of roots of the polynomial equation (12) by this behavior and Fig. 1.

this asymptotic behavior shows that this positive ψ corresponds to an asymptotically flat solution. This asymptotic behavior of $f(r)$ also explains that $\mathcal{M}$ corresponds to ADM mass.

In the last part of this subsection, we briefly check the behavior of our asymptotically flat root outside the asymptotic region. Let us use the graphical method with Fig. 1 again. Because $M(r)$ behaves as $0 \to M_{\max} \to 0$ when r moves $\infty \to r_{\max} \to r_0$, our $\psi(r)$ varies as $0 \to \psi_{\max} \to 0$. When r becomes smaller than r_0, $M(r)$ becomes negative and so $\psi(r)$ also takes negative values.

2.4. *Singularities*

In $\psi < 0$ or in $r < r_0$, our asymptotically flat solution has the curvature singularity. To confirm this, we examine the Kretschmann invariant

$$R_{\mu\nu\lambda\rho}R^{\mu\nu\lambda\rho} = f'' + 2n\frac{f'^2}{r^2} + 2n(n-1)\frac{(1-f)^2}{r^4}.$$

This value diverges at $r = 0$, and the singularity also exists where f' or f'' diverge. For example, f' has a term like $r^2\psi'$. From a derivative of (12), this can be estimated as $r^2\psi' = r^2M'/\partial_\psi\mathcal{P}$. Then, besides $r = 0$, $R_{\mu\nu\lambda\rho}R^{\mu\nu\lambda\rho}$ also diverges where the derivative of $\mathcal{P}[\psi]$ with respect to ψ becomes 0. If $\mathcal{P}[\psi]$ takes an extreme value at ψ_0, because $\mathcal{P}[\psi]$ is monotonically increasing in $\psi \geq 0$, such ψ_0 must be negative; i.e., there is a singularity at $r_s (< r_0)$. If $\mathcal{P}[\psi]$ is monotonically increasing for all ψ, there is a curvature singularity at $r = 0$. Therefore, whether $\mathcal{P}[\psi]$ has extreme values or not, our asymptotically flat branch has a curvature singularity somewhere in $0 \leq r < r_0$.

2.5. *Horizons*

Singularities must be wrapped by the event horizon from the standpoint of cosmic censorship. In this subsection, we consider horizons and present the condition for the existence of horizons.

Our asymptotically flat solution has an event horizon at $f(r) = 0$. This branch also satisfies $\mathcal{P}[\psi] = M(r)$, so horizons can be determined from

$$\begin{cases} 0 = 1 - r_H^2\psi_H \\ \mathcal{P}[\psi_H] = M(r_H) = \frac{\mathcal{M}}{r_H^{n+1}} - \frac{\mathcal{Q}^2}{r_H^{2n}}, \end{cases} \tag{15}$$

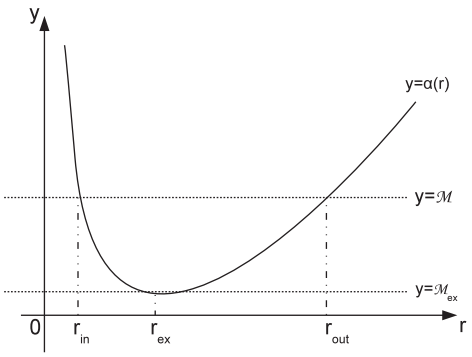

Fig. 3. The solid curve corresponds to $y = \alpha(r)$ and the dotted line is $y = \mathcal{M}$. In this figure, $y = \alpha(r)$ takes the extremal minimum at $r = r_{\rm ex}$. Because of (16), the cross points mean the horizon radii r_H.

where r_H is a horizon radius and ψ_H is defined as $\psi_H \equiv \psi(r_H)$. The first equation shows, if horizons exist, the corresponding ψ_H must be positive. Our $\psi(r)$ is positive in $r > r_0$, then r_H, if it exists, must satisfy $r_H > r_0$. As we have emphasized, the singularity exists somewhere in $r < r_0$. So we do not worry about the naked singularity if Eq. (15) have roots.

Here, we consider the criteria for the existence of roots of Eq. (15). Eliminating ψ_H by the first equation of (15), the second equation becomes the equation for r_H as follows:

$$\mathcal{P}\left[1/r_H^2\right] = \frac{\mathcal{M}}{r_H^{n+1}} - \frac{\mathcal{Q}^2}{r_H^{2n}}$$
$$\Leftrightarrow \mathcal{M} = \frac{\mathcal{Q}^2}{r_H^{n-1}} + \left(r_H^{n-1} + \sum_{m=2}^{k} \frac{\beta_m}{m} r_H^{n+1-2m}\right) \equiv \alpha(r_H). \tag{16}$$

The first term of $\alpha(r)$ is the negative power of r and its coefficient is positive. Under our assumption (13), because $n = 2k$ or $2k-1$, the other terms are positive powers of r and their coefficients are positive. Therefore, $y = \alpha(r)$ behaves as Fig. 3; $\alpha(r)$ diverges near $r = 0$, takes the extreme minimum at $r = r_{\rm ex}$ and monotonically increases in $r > r_{\rm ex}$. Then, we can denote that (16) has two roots when $\mathcal{M}$ is larger than $\mathcal{M}_{\rm ex}$ where

$$\mathcal{M}_{\rm ex} \equiv \alpha(r_{\rm ex}) = \frac{\mathcal{Q}^2}{r_{\rm ex}^{n-1}} + \left(r_{\rm ex}^{n-1} + \sum_{m=2}^{k} \frac{\beta_m}{m} r_{\rm ex}^{n+1-2m}\right). \tag{17}$$

In the two roots, the larger one corresponds to the outer horizon and we call this $r_{\rm out}$ hereafter. Note that $\alpha(r)$ only depends on $\mathcal{Q}$ except for the Lovelock couplings. Therefore, $r_{\rm ex}$ is determined when we fix $\mathcal{Q}$; this shows that $\mathcal{M}_{\rm ex}$ depends only on the charge.

Finally, we check the behaviors of some functions for later discussion. First, we examine the behavior of $M(r)$ outside of $r_{\rm out}$. The l.h.s. of the first equation of (16) is a monotonically decreasing function and the r.h.s. is monotonically increasing in $r < r_{\rm max}$ and monotonically decreasing in $r > r_{\rm max}$. Then, when (16) has two roots, it is forbidden that both of them are smaller than $r_{\rm max}$; at least, the larger root $r_{\rm out}$ must satisfy $r_{\rm out} > r_{\rm max}$. Hence,

$$M'(r) < 0 \quad (r > r_{\rm out}). \tag{18}$$

Then, in Fig. 1, while $r > r_{\rm out}$, the dotted line $y = M(r)$ falls monotonically as r becomes larger and so $\psi(r)$ decreases monotonically in this region. Therefore, from the relation $\psi' \partial_\psi \mathcal{P} = M'$, $\partial_\psi \mathcal{P}[\psi]$ satisfies

$$\partial_\psi \mathcal{P}[\psi] > 0 \tag{19}$$

when we consider the outside of $r_{\rm out}$.

3. Tensor-type perturbations

Thanks to the spherical symmetry of the background (7), tensor-type, vector-type, and scalar-type perturbations are decomposed and we can examine them separately. We have already examined the tensor perturbations in Ref. [34]. In this section, we briefly review our previous analysis. Note that we only consider the case when there exist horizons; i.e., $\mathcal{M} > \mathcal{M}_{\rm ex}$.

3.1. Master equation

Under tensor-type perturbations, there is no perturbation for the Maxwell field. Thus we only consider the gravitational perturbations

$$\delta g_{\mu\nu} = \left(\begin{array}{cc|c} 0 & 0 & 0 \\ 0 & 0 & 0 \\ \hline 0 & 0 & r^2 \phi \mathcal{T}_{ij} \end{array}\right). \tag{20}$$

In this expression, ϕ corresponds to the master variable. $\mathcal{T}_{ij}$ is the tensor harmonics, which is characterized by the traceless condition $\mathcal{T}^i{}_i = 0$, the divergence-free condition $\mathcal{T}_{ij}{}^{|j} = 0$, and the eigenequation $\mathcal{T}_{ij}{}^{|k}{}_{|k} = -(\ell(\ell+n-1)-2)\mathcal{T}_{ij}$. Note that $|$ is the covariant derivative for γ_{ij} and ℓ is the integer that satisfies $\ell \geq 2$.

Using the above metric perturbations, the first-order equation $\delta \mathcal{G}_i{}^j = 0$ reads [32,33]

$$T'\ddot{\phi} - f^2 T' \phi'' - f^2 T' \frac{(r^2 f T')'}{r^2 f T'} \phi' + \frac{\ell(\ell+n-1) f}{(n-2) r} T'' \phi = 0, \tag{21}$$

where $T(r)$ is

$$T(r) = r^{n-1} \partial_\psi \mathcal{P}[\psi], \tag{22}$$

which is always positive in $r > r_{\rm out}$ due to (19).

For this equation, as we have shown in Refs. [32–34], there exist ghost-like instabilities if T' has negative regions. For example, the coefficient of the kinetic term in (21) is proportional to T', so this term has the wrong sign while T' is negative. Thus, here we also assume $T'(r) > 0$ in $r > r_{\rm out}$ to avoid the ghost instability.

Under the ghost-free condition, we can change the normalization of ϕ as $\Psi(r) = \phi(r) r \sqrt{T'(r)}$. Using this variable, converting r to r^*, which is defined as $dr^*/dr = 1/f$, and performing a Fourier transformation like $\Psi \to \Psi e^{i\omega t}$, (21) is recast as

$$\mathcal{H}\Psi = \omega^2 \Psi, \tag{23}$$

where

$$\begin{aligned} \mathcal{H} &= -\partial_{r^*}^2 + V_g(r) \\ V_g(r) &= \frac{\ell(\ell+n-1) f}{(n-2) r} \frac{T''}{T'} + \frac{1}{r\sqrt{T'}} \partial_{r^*}^2 (r\sqrt{T'}). \end{aligned} \tag{24}$$

Equation (23) is a Schrödinger-type equation and its eigenvalue is ω^2. Thus, if this Schrödinger operator $\mathcal{H}$ has negative spectra, we can say charged Lovelock black holes are unstable under tensor-type perturbations.

3.2. *Stability analysis*

In this subsection, we show that "there exist negative spectra if T'' has negative regions in $r > r_{\rm out}$" when T' is always positive. To show this, we define the inner product as

$$(\chi_1, \chi_2) = \int_{-\infty}^{\infty} \chi_1^* \chi_2 dr^*, \tag{25}$$

and use the inequality

$$(\chi, \mathcal{H}\chi) \geq \omega_0^2 \cdot (\chi, \chi), \tag{26}$$

where ω_0^2 is the lower bound of the spectra and χ is an arbitrary smooth function with compact supports. From this inequality, we can show that there exist negative spectra if we find a function χ such that $(\chi, \mathcal{H}\chi)$ becomes negative under our assumptions.

We assume T'' has negative regions and define I as a closed set on such regions. Under these, we chose χ_0 as a smooth function that has a compact support on I. For this χ_0, $(\chi_0, \mathcal{H}\chi_0)$ is evaluated as

$$\begin{aligned}(\chi_0, \mathcal{H}\chi_0) &= \int_I dr^* \left[-\chi_0^* \partial_{r^*}^2 \chi_0 + V_g |\chi_0|^2\right] \\ &= \int_I |\partial_{r^*}\chi_0 - f\frac{d}{dr}\ln(r\sqrt{T'})\chi_0|^2 dr^* + \ell(\ell+n-1)\int_I \frac{f|\chi_0|^2}{(n-2)r}\frac{T''}{T'}dr^*. \end{aligned} \tag{27}$$

In this calculation, we use the Gauss divergence theorem and neglect the boundary terms because χ_0 is smoothly connecting to 0 at ∂I. In (27), the first term must be positive and the second integral is negative because we assume $T' > 0$ in $r > r_{\rm out}$ and $T'' < 0$ on I. Therefore, taking $\ell \to \infty$, $(\chi_0, \mathcal{H}\chi_0)$ must become negative. Because of (26), this means negative spectra exist in sufficiently large ℓ modes. Thus we can declare that black holes are unstable if T'' takes negative values somewhere in $r > r_{\rm out}$.

Inversely, it can also be shown that charged Lovelock black holes are stable if T'' is always positive in $r \geq r_{\rm out}$. As shown in Refs. [8–10], it is sufficient for the stability to show that $(\Phi, \mathcal{H}\Phi)$ is positive for ${}^\forall\Phi \in C_0^\infty(r^*)$. We can check this criterion by the same calculation of (27) and the positivity of T'', so we can say black holes are stable if T'' is always positive.

We want to summarize this section. To avoid the ghost instability, we must assume T' is always positive. Under this assumption, charged Lovelock black holes are stable if and only if T'' always takes positive values in $r > r_{\rm out}$. Hence, what we have to do is a probe of the behaviors of T' and T'', and we will check these in Sect. 6.

At the end of this section, we want to comment on T' in second-order Lovelock theory. We have already shown in our previous paper [34] that there is no ghost instability for this case. This can be checked by direct calculations: Eq. (14) leads to $T(r) = r^{n-1}\partial_\psi \mathcal{P}[\psi] = r^{n-1}\sqrt{1+2\beta_2 M(r)}$, then T' is calculated as

$$T' = \frac{r^{n-2}}{\sqrt{1+2\beta_2 M(r)}}\left[(n-1) + (n-3)\frac{\beta_2 \mathcal{M}}{r^{n+1}} + 2\frac{\beta_2 \mathcal{Q}^2}{r^{2n}}\right] > 0. \tag{28}$$

4. Vector-type perturbations

In this section, we examine vector-type perturbations. Here, we also assume $\mathcal{M} > \mathcal{M}_{\rm ex}$ for horizons and $T' > 0$ for no ghosts under tensor-type perturbations. We only consider the perturbations in $r > r_{\rm out}$. Under these assumptions, we derive the master equations for vector-type perturbations. Using these equations, we show that charged Lovelock black hole solutions are stable for vector-type perturbations when T' is always positive.

4.1. Gravitational perturbations

Firstly, we would like to consider metric perturbations. In this paper, we use the Regge–Wheeler gauge, in which the metric perturbations are expressed as

$$\delta g_{\mu\nu} = \left(\begin{array}{cc|c} 0 & 0 & h_1\mathcal{V}_i \\ 0 & 0 & h_2\mathcal{V}_i \\ \hline \text{sym} & \text{sym} & \mathbf{0} \end{array}\right). \tag{29}$$

In these, $\mathcal{V}_i$ is the vector harmonics that is characterized by the transverse condition $\mathcal{V}_i{}^{|i} = 0$ and the eigenequation $\mathcal{V}_i{}^{|l}{}_{|l} = -\kappa_v\mathcal{V}_i$ with $\kappa_v = \ell(\ell+n-1)-1$ $(\ell \geq 1)$.

For vector-type perturbations other than $\delta\mathcal{G}_t{}^i$, $\delta\mathcal{G}_r{}^i$ and $\delta\mathcal{G}_i{}^j$ are trivial. From the above metric, we can calculate the non-trivial components as

$$\begin{aligned}
\delta\mathcal{G}_t{}^i &= \left[\frac{(\kappa_v-(n-1))T'}{2(n-1)r^{n+2}}h_1 - \frac{f}{2r^{n+2}}\left\{r^3T\left(\left(\frac{h_1}{r^2}\right)' - \frac{\dot{h}_2}{r^2}\right)\right\}' + \frac{E^2}{r^2}h_1\right]\mathcal{V}^i, \\
\delta\mathcal{G}_r{}^i &= \left[\frac{(\kappa_v-(n-1))T'}{2(n-1)r^{n+2}}h_2 - \frac{1}{2r^{n+2}}\frac{r^3T}{f}\left\{\left(\frac{h_1}{r^2}\right)' - \frac{\dot{h}_2}{r^2}\right\}^{\cdot} + \frac{E^2}{r^2}h_2\right]\mathcal{V}^i, \\
\delta\mathcal{G}_i{}^j &= \frac{1}{2(n-1)}\left[-\frac{T'}{f}\dot{h}_1 + \left(fT'h_2\right)'\right]\left(\mathcal{V}_i{}^{|j} + \mathcal{V}_j{}^{|i}\right).
\end{aligned} \tag{30}$$

This is almost the same as the results of Refs. [32,33] except for the background electric field. This gap mainly arises from the difference of the identity

$$\left\{(rf'+2(1-f))T\right\}' = 2\frac{(r^nE)^2}{r^n}\,(\neq 0)\,.$$

4.2. Maxwell field perturbations

Next we examine the vector perturbations of the Maxwell field. We start from the perturbations of the vector potential

$$\delta A_\mu = (0,\ 0,\ C\mathcal{V}_i)^{\rm T}, \tag{31}$$

where $\mathcal{V}_i$ is the vector harmonics. Note that C is gauge invariant under the $U(1)$ gauge because there is no gauge freedom for vector perturbations. Using the above δA_μ, we can easily calculate the first order of the field strength as

$$\delta F_{ti} = \dot{C}\mathcal{V}_i,\ \delta F_{ri} = C'\mathcal{V}_i,\ \delta F_{ij} = C\left(\mathcal{V}_{j|i} - \mathcal{V}_{i|j}\right),\ \text{otherwise} = 0. \tag{32}$$

Here, we derive the evolution equation for the first-order variable C from the Maxwell equations. It is easy to check that the above field strength satisfies the identity $\delta F_{[\mu\nu;\lambda]} = 0$. Therefore,

$\delta(F_{\mu\nu}{}^{;\nu}) = 0$ is important for the evolution equation. In these equations, the $\mu = t, r$ components are trivial and the $\mu = i$ components read

$$\frac{1}{f}\ddot{C} - \frac{1}{r^{n-2}}\partial_r\left(r^{n-2} f \partial_r C\right) - r^2 E\left(\left(\frac{h_1}{r^2}\right)' - \frac{\dot{h}_2}{r^2}\right) + \frac{\kappa_v + (n-1)}{r^2} C = 0. \tag{33}$$

In order to obtain evolution equations for the gravitational field, we must calculate the first order of the energy momentum tensor (5). This tensor consists of $\delta F_{\mu\nu}$, $\delta g_{\mu\nu}$, and the background variables, so this tensor can be calculated from (32), (29), (7), and (8), and the results are as follows:

$$\begin{aligned}
\delta T_t{}^i &= \left[\frac{E^2}{r^2} h_1 + \frac{Ef}{r^2} C'\right] \mathcal{V}^i, \\
\delta T_r{}^i &= \left[\frac{E^2}{r^2} h_2 + \frac{E}{fr^2} \dot{C}\right] \mathcal{V}^i, \\
&\text{other components} = 0.
\end{aligned} \tag{34}$$

Then, from (30) and (34), the first-order Lovelock equations $\delta \mathcal{G}_\mu{}^\nu = \delta T_\mu{}^\nu$ read

$$\begin{aligned}
&\frac{T'}{2(n-1)r^{n+2}}\left(\kappa_v - (n-1)\right) h_1 - \frac{f}{2r^{n+2}}\left\{r^3 T\left(\left(\frac{h_1}{r^2}\right)' - \frac{\dot{h}_2}{r^2}\right)\right\}' = \frac{Ef}{r^2} C', \\
&\frac{T'}{2(n-1)r^{n+2}}\left(\kappa_v - (n-1)\right) h_2 - \frac{1}{2r^{n+2}}\frac{1}{f}\left\{r^3 T\left(\left(\frac{h_1}{r^2}\right)' - \frac{\dot{h}_2}{r^2}\right)\right\}^{\cdot} = \frac{E}{fr^2}\dot{C}, \\
&-\frac{T'}{f}\dot{h}_1 + \left(fT' h_2\right)' = 0.
\end{aligned} \tag{35}$$

4.3. *Master equations*

Now we are in a position to derive the master equations from (35) and (33). First of all, we treat the third equation of (35). From this equation we can define a new variable ϕ as

$$h_1 = \frac{f}{T'}\phi', \quad h_2 = \frac{1}{fT'}\dot{\phi}. \tag{36}$$

Substituting (36) into the first equation of (35) and integrating this with respect to r reads

$$2(Er^n)C + C_1(t) = \frac{\kappa_v - (n-1)}{n-1}\phi - r^3 T\left(\left(\frac{h_1}{r^2}\right)' - \frac{\dot{h}_2}{r^2}\right). \tag{37}$$

Here we use $(r^n E) = \text{const.}$ and $C_1(t)$ is a constant of the integral. In the same way, substituting (36) into the second equation of (35) and integrating this with respect to t leads to

$$2(Er^n)C + C_2(r) = \frac{\kappa_v - (n-1)}{n-1}\phi - r^3 T\left(\left(\frac{h_1}{r^2}\right)' - \frac{\dot{h}_2}{r^2}\right). \tag{38}$$

Comparing (37) with (38) shows that $C_1(t) = C_2(r) = \text{const.}$ and this constant can be absorbed into ϕ. Therefore, the three equations (35) are reduced into one equation

$$2(Er^n)C = \frac{\kappa_v - (n-1)}{n-1}\phi - r^3 T\left(\left(\frac{f}{r^2 T'}\phi'\right)' - \frac{1}{fr^2 T'}\ddot{\phi}\right). \tag{39}$$

In the same way as this substitution, (36) makes the Maxwell equation (33)

$$\frac{1}{f}\ddot{C} - \frac{1}{r^{n-2}}\partial_r\left(r^{n-2} f \partial_r C\right) + \frac{E}{rT}\left(2(Er^n)C - \frac{\kappa_v - (n-1)}{n-1}\phi\right) + \frac{\kappa_v + (n-1)}{r^2} C = 0. \tag{40}$$

As we have seen, ϕ determines the perturbations of the gravitational field and C determines those of the Maxwell field. Therefore, these are the master variables and (39) and (40) are the master equations for vector-type perturbations.

Finally, we would like to change these two equations into a Schrödinger equation with two components. To do so, we must change three points. Firstly, we change the normalization as

$$\Psi = \frac{\phi}{r\sqrt{T'}}, \quad \zeta = \sqrt{\frac{2(n-1)}{\kappa_v - (n-1)}} r^{(n-2)/2} C. \tag{41}$$

In this, we use the assumption that T' is always positive. Secondly, we switch the radial coordinate r to r^*. Finally, we perform a Fourier transformation like $\Psi \to \Psi e^{i\omega t}$ and $\zeta \to \zeta e^{i\omega t}$. Then, (39) and (40) become a Schrödinger equation with two components as

$$\mathcal{H}\begin{pmatrix}\Psi\\ \zeta\end{pmatrix} = \omega^2 \begin{pmatrix}\Psi\\ \zeta\end{pmatrix}, \tag{42}$$

where

$$\mathcal{H} = -\partial_{r^*}^2 + \begin{pmatrix} V_g(r) & V_c(r) \\ V_c(r) & V_{em}(r)\end{pmatrix} \tag{43}$$

and

$$\begin{aligned} V_g(r) &= \frac{\kappa_v - (n-1)}{n-1}\frac{fT'}{rT} + r\sqrt{T'}\partial_{r^*}^2 \frac{1}{r\sqrt{T'}}, \\ V_c(r) &= -2(Er^n)\sqrt{\frac{\kappa_v - (n-1)}{2(n-1)}}\frac{f\sqrt{T'}}{r^{(n+2)/2}T}, \\ V_{em}(r) &= (\kappa_v + (n-1))\frac{f}{r^2} + 2(Er^n)^2\frac{f}{r^{n+1}T} + r^{-(n-2)/2}\partial_{r^*}^2 r^{(n-2)/2}. \end{aligned} \tag{44}$$

Note that these equations are not decomposed due to the higher curvature collections. In the Einstein limit, owing to $T(r) = r^{n-1}$, the above potential matrix can be diagonalized by constant eigenvectors. This indicates that our Schrödinger equation can be decomposed into two equations by taking suitable linear combinations of ψ and ζ. In fact, we can do so by using the combinations $\alpha_\pm \psi - \zeta$ with

$$\alpha_\pm = \frac{(n^2-1)\mathcal{M} \pm \sqrt{(n^2-1)^2\mathcal{M}^2 + 8(\kappa_v - (n-1))(r^nE)^2}}{2(r^nE)\sqrt{2(\kappa_v - (n-1))}}, \tag{45}$$

which is consistent with Ref. [11]. In contrast with this, because $T(r)$ is more complicated in general Lovelock theory, we must consider the above coupling system.

4.4. *Stability analysis*

In this subsection, we show that the Schrödinger equation (42) has no negative eigenvalue state.

In order to show this, for $\vec{\Psi} = (\Psi,\ \zeta)^T$, we define the inner product as

$$(\vec{\Psi}_1,\ \vec{\Psi}_2) = \int_{-\infty}^{\infty} dr^* \left[\Psi_1^* \Psi_2 + \zeta_1^* \zeta_2\right]. \tag{46}$$

Here, we prove that charged Lovelock black holes are stable for vector-type perturbations. In order to show this, we prove that $\mathcal{H}$ is an essentially self-adjoint, positive-definite operator. For this, because $\mathcal{H}$ with $C_0^\infty(r^*) \times C_0^\infty(r^*)$ is a symmetric operator, it is sufficient to check that this operator is positive-definite [8–10].

We assume $\vec{\Psi}_0 \in C_0^\infty(r^*) \times C_0^\infty(r^*)$, then $(\vec{\Psi}_0, \mathcal{H}\vec{\Psi}_0)$ can be estimated as

$$
\begin{aligned}
(\vec{\Psi}_0, \mathcal{H}\vec{\Psi}_0) &= \int dr^* \Big[-\psi_0^* \partial_{r^*}^2 \psi_0 - \zeta_0^* \partial_{r^*}^2 \zeta_0 \\
&\quad + V_g |\psi_0|^2 + V_c(\psi_0^* \zeta_0 + \psi_0 \zeta_0^*) + V_{em} |\zeta_0|^2 \Big] \\
&= \int dr^* \left[\left| \partial_{r^*} \psi_0 + \left(\partial_{r^*} \ln(r\sqrt{T'}) \right) \psi_0 \right|^2 + \left| \partial_{r^*} \zeta_0 - \frac{n-2}{2} \frac{f}{r} \zeta_0 \right|^2 \right. \\
&\quad + \frac{\kappa_v - (n-1)}{n-1} \frac{f T'}{rT} |\psi_0|^2 + 2(Er^n)^2 \frac{f}{r^{n+1} T} |\zeta_0|^2 \\
&\quad + (\kappa_v + (n-1)) \frac{f}{r^2} |\zeta_0|^2 \\
&\quad \left. - \sqrt{\frac{2(\kappa_v - (n-1))}{n-1}} (Er^n) \frac{f\sqrt{T'}}{r^{(n+2)/2} T} (\psi_0^* \zeta_0 + \psi_0 \zeta_0^*) \right] \\
&= \int dr^* \left[\left| \partial_{r^*} \psi_0 + \left(\partial_{r^*} \ln(r\sqrt{T'}) \right) \psi_0 \right|^2 + \left| \partial_{r^*} \zeta_0 - \frac{n-2}{2} \frac{f}{r} \zeta_0 \right|^2 \right. \\
&\quad + \frac{f}{rT} \left| \frac{\sqrt{2}(Er^n)}{r^{n/2}} \zeta_0 - \sqrt{\frac{\kappa_v - (n-1)}{n-1}} \sqrt{T'} \psi_0 \right|^2 \\
&\quad \left. + (\kappa_v + (n-1)) \frac{f}{r^2} |\zeta_0|^2 \right] > 0,
\end{aligned}
\tag{47}
$$

where we use the Gauss theorem in the second equality and neglect the boundary terms because Ψ_0 and ζ_0 are in $C_0^\infty(r^*)$. This calculation shows that $\mathcal{H}$ with $C_0^\infty(r^*) \times C_0^\infty(r^*)$ is positive-definite. Then, since $\mathcal{H}$ with $C_0^\infty \times C_0^\infty$ is essentially self-adjoint, $\mathcal{H}$ can be uniquely extended to a self-adjoint positive-definite operator, so there is no instability under vector-type perturbations.

5. Scalar-type perturbations

In this section, we derive the master equations and present conditions for instability under scalar-type perturbations. In this section, we assume that $\mathcal{M} > \mathcal{M}_{\rm ex}$ and also assume that T' is always positive outside $r_{\rm out}$.

5.1. Gravitational perturbations

Firstly, we consider the metric perturbations. In this paper, we take the Zerilli gauge in which metric perturbations are described as

$$
\delta g_{\mu\nu} = \left(\begin{array}{cc|c} f H_0 \mathcal{Y} & H_1 \mathcal{Y} & 0 \\ \text{sym} & H\mathcal{Y}/f & 0 \\ \hline \text{sym} & \text{sym} & r^2 K \mathcal{Y} \gamma_{ij} \end{array} \right),
\tag{48}
$$

where $\mathcal{Y}$ is the scalar harmonics that is characterized by the eigenequation ${\mathcal{Y}_{|l}}^{|l} = -\kappa_s \mathcal{Y}$ with $\kappa_s = \ell(\ell + n - 1)$ and $\ell = 0, 1, 2, \cdots$.

To derive the master equation, it is sufficient that we calculate $\delta\mathcal{G}_i^j$ $(i \neq j)$, $\delta\mathcal{G}_t^r$, $\delta\mathcal{G}_t^t$, $\delta\mathcal{G}_r^i$, and $\delta\mathcal{G}_r^r$ [29–31]. By the above metric perturbations, we can derive the following results [32,33]:

$$
\begin{aligned}
\delta\mathcal{G}_i{}^j &= \frac{1}{2(n-1)r^n}(T'H_0 - T'H - rT''K)\mathcal{Y}^{|j}{}_{|i}, \\
\delta\mathcal{G}_t{}^r &= \frac{fT}{2r^{n+1}}\left[-\kappa_s H_1 + n\left\{\left(r - \frac{r^2 f'}{2f}\right)K + r^2 K' - rH\right\}^{\cdot}\right]\mathcal{Y}, \\
\delta\mathcal{G}_t{}^t &= \frac{1}{2r^{n+1}}\left[\{-\kappa_s T - nr(fT)'\}H - nrfTH' + (n-\kappa_s)rT'K\right. \\
&\quad \left. + \left\{\frac{nr^2 f'T}{2} + nf(r^2T)'\right\}K' + nr^2 fTK''\right]\mathcal{Y}, \\
\delta\mathcal{G}_r{}^i &= \frac{1}{2r^{n+1}}\left[\left(T' + \frac{f'T}{2f}\right)H - rT'K' + \left(\frac{f'T}{2f} - \frac{T}{r}\right)H_0 + TH_0' - \frac{T}{f}\dot{H}_1\right]\mathcal{Y}^{|i}, \\
\delta\mathcal{G}_r{}^r &= \frac{1}{2r^{n+1}}\left[2nrT\dot{H}_1 - \frac{nr^2T}{f}\ddot{K} + (n-\kappa_s)rT'K + \left(nr^2 fT' + \frac{nr^2 f'T}{2}\right)K'\right. \\
&\quad \left. - nr(fT)'H + \kappa_s TH_0 - nrfTH_0'\right]\mathcal{Y}.
\end{aligned}
\tag{49}
$$

These are the same as our previous calculation for neutral black holes except for the detailed expression of $f(r)$.

5.2. *Scalar perturbations for the Maxwell field*

Next, we examine the scalar perturbations for the Maxwell field. We start from perturbations of the field strength with $U(1)$ gauge invariance. We describe this as

$$
\delta F_{\mu\nu} = \left(\begin{array}{cc|c} 0 & X\mathcal{Y} & Y\mathcal{Y}_{|i} \\ -X\mathcal{Y} & 0 & Z\mathcal{Y}_{|i} \\ \hline \multicolumn{2}{c|}{\text{anti sym.}} & 0 \end{array}\right), \tag{50}
$$

where $\mathcal{Y}$ is the scalar harmonics. Note that $\delta F_{ij} = 0$ because we cannot construct antisymmetric tensors from scalar functions.

The starting point (50) enables us to calculate the identity $\delta F_{[\mu\nu;\lambda]} = 0$, Maxwell equations $\delta(F^{\mu\nu}{}_{;\nu}) = 0$, and the energy momentum tensor $\delta T_\mu{}^\nu$. Firstly, we check the identity. It is easy to show that the components other than $(\mu,\ \nu,\ \lambda) = (t,\ r,\ i)$ are trivial and that the non-trivial component reads

$$
X = Y' - \dot{Z}. \tag{51}
$$

Secondly, we calculate the Maxwell equations $\delta(F^{\mu\nu}{}_{;\nu}) = 0$. From the $\mu = t$ component, we can obtain the equation

$$
\frac{1}{2}(r^n E)\partial_r(H_0 - H + nK) - \partial_r(r^n X) + \frac{\kappa_s r^{n-2}}{f}Y = 0. \tag{52}
$$

In the same way, the $\mu = r$ component reads

$$
\frac{1}{2}(r^n E)\partial_t(H_0 - H + nK) - \partial_t(r^n X) + \kappa_s r^{n-2} fZ = 0 \tag{53}
$$

and $\mu = i$ components read

$$
\partial_r(r^{n-2} fZ) - \partial_t\left(\frac{r^{n-2}}{f}Y\right) = 0. \tag{54}
$$

Before calculating $\delta T_\mu{}^\nu$, let us reduce the four equations (51)–(54) into one equation. From (54), we can define a new variable B as

$$Z = \frac{1}{r^{n-2} f}\dot{B}, \quad Y = \frac{f}{r^{n-2}}B'. \tag{55}$$

Substituting (55) into (52) and integrating this with respect to r, (52) becomes

$$\frac{1}{2}(r^n E)(H_0 - H + nK) - r^n X + \kappa_s B + C_1(t) = 0,$$

where $C_1(t)$ is a constant of the integral. We use $r^n E = \text{const.}$ in this integral. In the same way, (53) becomes

$$\frac{1}{2}(r^n E)(H_0 - H + nK) - r^n X + \kappa_s B + C_2(r) = 0.$$

Here $C_2(r)$ is also a constant of the integral. Then, a comparison with above two equations leads to $C_1(t) = C_2(r) = \text{const.}$ and so this term can be absorbed into B. Therefore,

$$\frac{1}{2}(r^n E)(H_0 - H + nK) - r^n X + \kappa_s B = 0. \tag{56}$$

Equations (55) and (56) suggest that B (and gravitational perturbations) determines the perturbations of the Maxwell field, so we can say B is the master variable for the Maxwell field. The evolution equation for the master variable B can be derived by eliminating X in (56) with (51) and (55). The result is

$$\frac{r^2}{f}\partial_t^2 B - r^n \partial_r \frac{f}{r^{n-2}}\partial_r B + \kappa_s B + \frac{(r^n E)}{2}(H_0 - H + nK) = 0. \tag{57}$$

Finally, for the first-order perturbations of the Lovelock equations, we calculate the first order of the energy momentum tensor (5). Equation (5), the background electric field $E(r)$, the metric perturbations (48), and the perturbations of the Maxwell field (50) yield

$$\begin{aligned}
&\delta T_t{}^t = \delta T_r{}^r = \left[EX + \frac{1}{2}E^2(H - H_0)\right]\mathcal{Y} = \left[\frac{\kappa_s}{r^n}B + \frac{n}{2}EK\right]\mathcal{Y}, \\
&\delta T_t{}^r = 0, \quad \delta T_r{}^i = \frac{E}{r^2 f}Y\mathcal{Y}^{|i} = \frac{E}{r^n}B'\mathcal{Y}^{|i}, \quad \delta T_i{}^j = 0\ (i \neq j).
\end{aligned} \tag{58}$$

Note that we use the relation (56) in the (t, t), (r, r) components and that we also use the relation (55) in the (r, i) components.

5.3. *Master equations*

From the first-order Lovelock tensor (49) and that of the energy momentum tensor (58), the components we concentrate on are

$$T'H_0 - T'H = rT''K, \tag{59}$$

$$-\kappa_s H_1 + n\left\{\left(r - \frac{r^2 f'}{2f}\right)K + r^2 K' - rH\right\}^{\cdot} = 0, \tag{60}$$

$$(n-\kappa_s)rT'K+\left(\frac{nr^2f'T}{2}+nf(r^2T)'\right)K'+nr^2fTK''$$
$$-(\kappa_sT+nr(fT)')H-nrfTH'=2r^{n+1}E\left(\frac{\kappa_s}{r^n}B+\frac{n}{2}EK\right), \tag{61}$$

$$\left(T'+\frac{f'T}{2f}\right)H-rT'K'+\left(\frac{f'T}{2f}-\frac{T}{r}\right)H_0+TH_0'-\frac{T}{f}\dot{H}_1=2ErB', \tag{62}$$

$$(n-\kappa_s)rT'K+\left(nr^2fT'+\frac{nr^2f'T}{2}\right)K'-nr(fT)'H$$
$$+\kappa_sTH_0-nrfTH_0'+2nrT\dot{H}_1-\frac{nr^2T}{f}\ddot{K}=2r^{n+1}E\left(\frac{\kappa_s}{r^n}B+\frac{1}{2}nEK\right). \tag{63}$$

From now on, we would like to construct the master equation. In order to derive this, we must define the master variable ϕ and denote the gravitational perturbations by this ϕ. In the same way as the analysis for neutral black holes [32,33], we define the master variable ϕ as

$$H_1=\frac{r}{f}\left(\dot{\phi}+\dot{K}\right). \tag{64}$$

Then, from (59), (60), and (61), we can express H_0, H, and K as follows [32,33]:

$$H_0=H+\frac{rT''}{T'}K,$$
$$H=-\frac{\kappa_s}{nf}\phi+rK'-\frac{\mathcal{A}(r)}{2nf}K,$$
$$K=\frac{4nrfE}{\mathcal{A}T}B-\frac{2}{\mathcal{A}}\left[nrf\phi'+\left(\kappa_s+nrf\frac{T'}{T}\right)\phi\right], \tag{65}$$

where

$$\mathcal{A}(r)=2\kappa_s+nrf'-2nf. \tag{66}$$

The above equations show that the two variables ϕ and B express the perturbative variables and so these are the master variables. Therefore, we must construct the evolution equations for these variables in order to examine the stability of the background solution. That for B has already been derived as (57), but this includes the metric perturbations. Thus, substituting (65) into (57), we obtain

$$\ddot{B}-f^2B''+f^2\left(\ln\left(\frac{r^{n-2}}{f}\right)\right)'B'+\frac{\kappa_sf}{r^2}B$$
$$+\frac{(r^nE)f}{2r\mathcal{A}T}\left(\ln(r^nT')\right)'\times\left(4nrEfB-2nrfT\phi'-2(\kappa_sT+nrfT')\phi\right)=0. \tag{67}$$

The evolution equation for ϕ is derived from $nrf\times(62)+(63)$ with (65) (see Refs. [32,33]) and the result is

$$\ddot{\phi}-f^2\phi''+f^2\left(\ln\left(\frac{\mathcal{A}^2}{r^2fT'}\right)\right)'\phi'+\frac{f}{nr^2T}\left[\left(2\frac{(\mathcal{A}T)'}{\mathcal{A}T}-\frac{T''}{T'}\right)(\kappa_srT+nr^2fT')-n(r^2fT')'\right]\phi$$
$$+\left[-f\frac{4\kappa_s(Er^n)}{nr^{n+1}T}+\frac{2f^2(Er^n)}{r^nT}\left(\ln\left(\frac{fT'}{r^{n-2}(\mathcal{A}T)^2}\right)\right)'\right]B=0. \tag{68}$$

These two coupled equations (67) and (68) determine the behaviors of ϕ and B. These two functions determine all perturbative variables, so these two equations are the master equations.

Here, we derive a Schrödinger equation with two components like (42) from these two equations. In contrast with the case for vector-type perturbations, it is more complicated because there is ϕ' in the

evolution equation for B. Therefore, in order to transform these equations into a Schrödinger-type equation, we must eliminate this ϕ'. For this, we must consider linear combinations of the master variables ϕ and B. For example, the following combinations are fit for our purpose:

$$\Psi \equiv \frac{r\sqrt{T'}}{\mathcal{A}}\phi, \quad \zeta = \frac{1}{r^{(n-2)/2}\sqrt{n(\kappa_s - n)}}\left(B - \frac{n(r^n E)}{\mathcal{A}}\phi\right). \tag{69}$$

By using these variables and the tortoise coordinate r^*, we can obtain

$$\mathcal{H}\begin{pmatrix}\Psi\\ \zeta\end{pmatrix} = \omega^2\begin{pmatrix}\Psi\\ \zeta\end{pmatrix}, \tag{70}$$

where

$$\mathcal{H} = -\partial_{r^*}^2 + \begin{pmatrix}V_g(r) & V_c(r)\\ V_c(r) & V_{em}(r)\end{pmatrix} \tag{71}$$

and

$$\begin{aligned}
V_g(r) &= \kappa_s \frac{f}{nr}\left(4(\kappa_s - n)\frac{T'}{\mathcal{A}T} - \frac{T''}{T'}\right)\\
&\quad + \frac{2n(r^n E)^2 f^2}{\mathcal{A}T r^n}\left(\ln\left(\frac{fT'}{r^{n-2}(\mathcal{A}T)^2}\right)\right)' + \frac{\mathcal{A}T}{r\sqrt{T'}} f\partial_r\left(f\partial_r \frac{r\sqrt{T'}}{\mathcal{A}T}\right),\\
V_c(r) &= \sqrt{\frac{\kappa_s - n}{n}}\frac{\sqrt{T'}}{r^{n/2}\mathcal{A}}\left[-\kappa_s \frac{4(r^n E)f}{rT} + \frac{2n(r^n E)f^2}{T}\left(\ln\left(\frac{fT'}{r^{n-2}(\mathcal{A}T)^2}\right)\right)'\right],\\
V_{em}(r) &= f r^{(n-2)/2}\partial_r\left(f\partial_r \frac{1}{r^{(n-2)/2}}\right)\\
&\quad + \kappa_s \frac{f}{r^2}\left(1 + \frac{4(Er^n)^2}{\mathcal{A}T r^{n-1}}\right) + \frac{2n(r^n E)^2 f^2}{r^n \mathcal{A}T}\left(\ln\left(\frac{r^{2n-2}(\mathcal{A}T)^2}{f}\right)\right)'.
\end{aligned} \tag{72}$$

Here, we perform a Fourier transformation like $\Psi \to \Psi e^{i\omega t}$ and $\zeta \to \zeta e^{i\omega t}$. Note that, in the Einstein limit, we can decompose the above equation into two Schrödinger equations by taking linear combinations like $\psi - \alpha_\pm \zeta$, where

$$\alpha_\pm = \frac{1}{4(r^n E)}\sqrt{\frac{n(n-1)}{\kappa_s - n}}(n+1)\left(\mathcal{M} \pm \sqrt{\mathcal{M}^2 + \frac{16(\kappa_s - n)(r^n E)^2}{n(n-1)(n+1)^2}}\right). \tag{73}$$

This is consistent with Ref. [11]. We can do this because $T(r) = r^{n-1}$ in Einstein theory. In contrast with this, because $T(r)$ is more complicated in general Lovelock theory, we must consider the above coupling system.

5.4. *Conditions for instabilities*

In this subsection, we show the criterion for instability under scalar-type perturbations.

Here, we show that "if $2T'^2 - TT''$ takes negative values somewhere in $r > r_{\rm out}$, charged Lovelock black holes show instability" when T' is always positive. In order to show this, we here also define the inner product as

$$(\vec{\Psi}_1,\ \vec{\Psi}_2) = \int_{-\infty}^{\infty} dr^* \left[\Psi_1^* \Psi_2 + \zeta_1^* \zeta_2\right], \tag{74}$$

where $\vec{\Psi} = (\Psi,\ \zeta)^T$. For this proof, it is convenient to use the following inequality: for any test function $\vec{\Psi}_{\rm test} \in C_0^\infty \times C_0^\infty$, the lower bound of the spectra for $\mathcal{H}$ with $C_0^\infty \times C_0^\infty$ satisfies

$$\omega_0^2 \cdot (\vec{\Psi}_{\rm test},\ \vec{\Psi}_{\rm test}) \leq (\vec{\Psi}_{\rm test},\ \mathcal{H}\vec{\Psi}_{\rm test}). \tag{75}$$

This inequality suggests that there exist instabilities if we can find a trial function $\vec{\Psi}_{\rm test}$ that satisfies $(\vec{\Psi}_{\rm test},\ \mathcal{H}\vec{\Psi}_{\rm test}) < 0$.

We assume that $2T'^2 - TT''$ has negative regions and define I as a closed set in the region $2T'^2 - TT'' < 0$. Then, we choose a trial function as $\vec{\Psi}_{\rm test} = (\Psi_0,\ 0)^T$, where Ψ_0 is a sufficiently smooth function with a compact support on I. Using this test function, $(\vec{\Psi}_{\rm test},\ \mathcal{H}\vec{\Psi}_{\rm test})$ is evaluated as

$$\begin{aligned}(\vec{\Psi}_{\rm test},\ \mathcal{H}\vec{\Psi}_{\rm test}) &= \int_I dr^* \left[-\Psi_0^* \partial_{r^*}^2 \Psi_0 + V_g(r)|\Psi_0|^2\right] \\ &= \int_I dr^* \left[\left|\partial_{r^*}\Psi_0 + f\left(\partial_r \ln \frac{\mathcal{A}T}{r\sqrt{T'}}\right)\Psi_0\right|^2 + 2\kappa_s \frac{f}{nr}\left(2(\kappa_s - n)\frac{T'}{\mathcal{A}T} - \frac{T''}{2T'}\right)|\Psi_0|^2 \right. \\ &\quad \left. + \frac{2n(r^n E)^2 f^2}{\mathcal{A}T r^n}\left(\ln\left(\frac{fT'}{r^{n-2}(\mathcal{A}T)^2}\right)\right)'|\Psi_0|^2\right]. \end{aligned} \tag{76}$$

Note that we neglect the boundary terms in the second equality because Ψ_0 is zero at the boundary of I. Furthermore, using the relation

$$\mathcal{A}T = 2(\kappa_s - n)T - nr^{n+2}M'(r),$$

the second line of the last equation can be evaluated as

$$\begin{aligned}&\int_I dr^* \left[2\kappa_s \frac{f}{nr}\left(2(\kappa_s - n)\frac{T'}{\mathcal{A}T} - \frac{T''}{2T'}\right)|\Psi_0|^2\right] \\ &= \int_I dr^* \left[2\kappa_s \frac{f}{nr}\left(\frac{2(\kappa_s - n)}{2(\kappa_s - n) - nr^{n+2}\frac{M'(r)}{T}}\frac{T'}{T} - \frac{T''}{2T'}\right)|\Psi_0|^2\right] \\ &< \int_I dr^* \left[2\kappa_s \frac{f}{nr}\left(\frac{T'}{T} - \frac{T''}{2T'}\right)|\Psi_0|^2\right] = \kappa_s \int_I dr^* \left[\frac{f}{nrTT'}\left(2T'^2 - TT''\right)|\Psi_0|^2\right], \end{aligned} \tag{77}$$

where we use the positivity of T and T' and also use Eq. (18) in the inequality. Then $(\vec{\Psi}_{\rm test},\ \mathcal{H}\vec{\Psi}_{\rm test})$ satisfies the following inequality;

$$\begin{aligned}(\vec{\Psi}_{\rm test},\ \mathcal{H}\vec{\Psi}_{\rm test}) < \int_I dr^* \left[\left|\partial_{r^*}\Psi_0 + f\left(\partial_r \ln \frac{\mathcal{A}T}{r\sqrt{T'}}\right)\Psi_0\right|^2 \right. \\ \left. + \frac{2n(r^n E)^2 f^2}{\mathcal{A}T r^n}\left(\ln\left(\frac{fT'}{r^{n-2}(\mathcal{A}T)^2}\right)\right)'|\Psi_0|^2\right] \\ + \kappa_s \int_I dr^* \left[\frac{f}{nrTT'}\left(2T'^2 - TT''\right)|\Psi_0|^2\right]. \end{aligned} \tag{78}$$

In this equation, the second integral must be negative under our assumptions. Therefore the second integral of (78) tends to $-\infty$ when $\kappa_s = \ell(\ell + n - 1) \to \infty$. In contrast with this result, the first

integral of (78) converges when $\ell \to \infty$ like

$$\int_I dr^* \left[\left| \partial_{r^*}\Psi_0 + f\left(\partial_r \ln \frac{\mathcal{A}T}{r\sqrt{T'}}\right)\Psi_0 \right|^2 + \frac{2n(r^nE)^2 f^2}{\mathcal{A}Tr^n}\left(\ln\left(\frac{fT'}{r^{n-2}(\mathcal{A}T)^2}\right)\right)' |\Psi_0|^2 \right]$$
$$\to \int_I dr^* \left[\left| \partial_{r^*}\Psi_0 + f\left(\partial_r \ln \frac{T}{r\sqrt{T'}}\right)\Psi_0 \right|^2 \right]. \tag{79}$$

This is because the integrands converge uniformly on I like

$$\partial_{r^*}\Psi_0 + f\left(\partial_r \ln \frac{\mathcal{A}T}{r\sqrt{T'}}\right)\Psi_0 \to \partial_{r^*}\Psi_0 + f\left(\partial_r \ln \frac{T}{r\sqrt{T'}}\right)\Psi_0,$$
$$\frac{2n(r^nE)^2 f^2}{\mathcal{A}Tr^n}\left(\ln\left(\frac{fT'}{r^{n-2}(\mathcal{A}T)^2}\right)\right)' |\Psi_0|^2 \to 0, \tag{80}$$

where these uniform convergences are supported by the theorem that continuity functions on closed sets have maximum and minimum values. Therefore, summarizing these results, we can denote that the r.h.s. of (78) tends to $-\infty$ as $\ell \to \infty$. This means that the lower bound of the spectra is negative in sufficiently large ℓ modes and so the background solution shows instability for these modes.

We would like to summarize this section. We assume that $T' > 0$ in $r > r_{\rm out}$. Under this assumption, we have derived the master equations. We can unify these equations as a Schrödinger equation with two components. We show that this Schrödinger operator has negative spectra when $2T'^2 - TT''$ has negative regions. Therefore, we can denote that $2T'^2 - TT''$ is crucial for the stability of charged Lovelock black holes. This criterion is the same as that for neutral cases [32,33].

We have not shown the inverse statement so far. Thus, even if $2T'^2 - TT''$ is always positive, we cannot declare that this black hole is stable. For example, in the Einstein case, $T(r)$ is r^{n-1}, so $2T'^2 - TT'' = n(n-1)r^{2(n-2)} > 0$. Thus we cannot say anything for the Einstein case. In the same way, in 6 dimensions, this function can be evaluated as

$$2T'^2 - TT'' = 3\frac{r^3(\beta_2\mathcal{M} - 2r^5)^2 + 8\beta_2\mathcal{Q}^2(\beta_2\mathcal{M} + 3r^5)}{r^9(1 + 2\beta_2 M(r))} > 0, \tag{81}$$

so we cannot say anything for scalar perturbations in 6 dimensions .

6. Numerical results

In Sects. 3 and 5, we have shown that the behavior of $T(r)$ is crucial for the instability. In detail, T' is critical for ghosts, T'' is for tensor perturbations, and $2T'^2 - TT''$ is for scalar perturbations. In this section, we check the behaviors of these functions. For neutral cases, we can examine them analytically because we can reduce these functions into polynomial functions of ψ [32,33]. However, such reductions cannot be performed in charged cases. Therefore, we numerically check the behaviors of T', T'', and $2T'^2 - TT'$ for various $(|\mathcal{Q}|, \mathcal{M})$ with some Lovelock couplings.

In numerical calculations, we must use dimensionless parameters. So far we have discussed results using the unit $\beta_1 = 1$; in this unit, we cannot fix the scale of the length. As in our previous paper [34], we here also use β_2 to fix this scale. This constant has a dimension of the length squared. Therefore, we can relate r, ψ, $\mathcal{M}$, $\mathcal{Q}$, and the Lovelock couplings β_ms to the dimensionless parameters as follows:

$$\tilde{r} \equiv r/\sqrt{\beta_2}, \quad \tilde{\psi} \equiv \beta_2\psi, \quad \mu \equiv \beta_2^{-(n-1)/2}\mathcal{M}, \quad Q \equiv \beta_2^{-(n-1)/2}\mathcal{Q}, \quad c_m \equiv \frac{\beta_m}{\beta_2^{m-1}}.$$

Hereafter, we show some results for 5–8 dimensions. The strategy for our numerical calculation is basically same as that in our previous paper, except for checking $2T'^2 - TT''$ [34]. Note that $\mu_{\rm ex}$ is the dimensionless extreme mass parameter, which can be calculated from (17). $\mu_{\rm tensor}$ is the border between stability and instability for tensor-type perturbations and $\mu_{\rm scalar}$ corresponds to that for scalar-type perturbations.

6.1. 5 dimensions

As we have mentioned above, we use β_2 to fix the scale of the length. Thus we need not regard the Lovelock couplings in 5 dimensions.

We present the numerical results for 5 dimensions in Fig. 4. For this figure, we check the region where $\mu_{\rm ex}(|Q|) \sim \mu_{\rm ex}(|Q|) + 3$ for each $|Q|$ and the mesh size is $d\mu = dQ = 10^{-3}$.

As shown in our previous papers [32,33], the tensor-unstable region lies thinly on the extreme mass $\mu_{\rm ex}(|Q|)$ and $\mu_{\rm tensor}(|Q|)$ converges to 0.5 when $|Q| \to 0$. In this limit, $\mu_{\rm ex}$ also converges to this value. Note that this thin region is over at $|Q| \sim 3$, which has been checked in our previous analysis. In contrast with the tensor-unstable region, for scalar-type perturbations, the unstable mass range is relatively wide and this unstable region localizes near the μ-axis; the upper line of this region is approximately expressed as $\mu \sim 2.914$ and this region suddenly disappears near $|Q| \sim 0.62$. For the ghost instability, we have already checked the positivity of T' in (28).

Thus, roughly speaking, charged Lovelock black holes with $\mu < 2.914$ show instability for scalar modes when $|Q| < 0.62$; if $0.62 < |Q| < 3$, nearly extreme black holes are unstable for tensor-type perturbations. We cannot detect the instability when the black hole has more charge.

6.2. 6 dimensions

In 6 dimensions, as in the 5-dimensional case, we need not alter the Lovelock coefficients.

We present the numerical results for 6 dimensions in Fig. 5. As we showed in Sect. 3, T' is always positive, so there is no ghost. It was also mentioned in Sect. 5 that $2T'^2 - TT''$ is positive-definite in 6 dimensions, which means that we cannot find the instability for scalar-type perturbations. Thus we can only detect instability under tensor perturbations and the results are the same as for our previous analysis [34]: like the tensor-unstable region in 5vdimensions, this region exists slightly on $\mu_{\rm ex}(|Q|)$

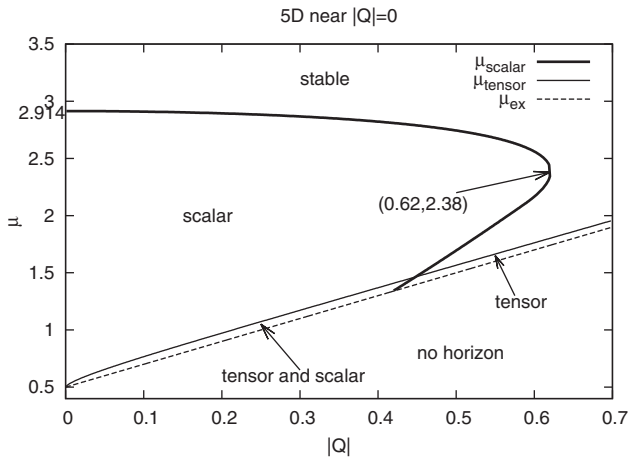

Fig. 4. Numerical results in 5 dimensions. The scalar-unstable region localizes near the μ-axis and there exists a slight gap between $\mu_{\rm tensor}$ and $\mu_{\rm ex}$. This gap is about $O(10^{-1})$. Notice that "stable" means that neither T'' nor $2T'^2 - TT''$ have a negative region. This is same for the following figures.

and disappears at $|Q| \sim 3.28$. However, there also exists a difference: $\mu_{\rm tensor}$ converges to 0.27 in $|Q| \to 0$ while $\mu_{\rm ex} \to 0$. Therefore, we can say that black holes with $\mu \sim \mu_{\rm ex}$ show instability under tensor-type perturbations when $0 \leq |Q| < 3.28$. In particular, in contrast with the 5-dimensional case, black holes also show instability in neutral cases.

6.3. 7 dimensions

We present the numerical results for 7 dimensions in Fig. 6. This figure is calculated with $c_3 = 0.2$ in 7 dimensions. For this figure, we check the region where $\mu_{\rm ex}(|Q|) \sim \mu_{\rm ex}(|Q|) + 4.2$ for each $|Q|$ and the mesh size is $d\mu = dQ = 10^{-3}$.

This diagram is almost the same as that for the 5-dimensional case; the tensor-unstable region clings to $\mu_{\rm ex}(|Q|)$, as does the scalar region to the μ-axis. Our previous analysis shows that a tensor-unstable region exists in $0 < |Q| < 4.695$ [34]. The upper bound of the scalar-unstable region is

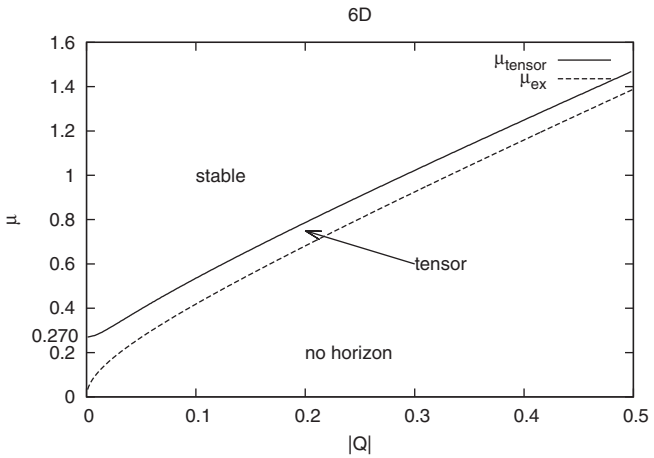

Fig. 5. Numerical results in 6 dimensions. Unlike the 5-dimensional case, there are no scalar-unstable regions, due to Eq. (81). The tensor-unstable region lies slightly on the extreme line $\mu_{\rm ex}(|Q|)$. This region ends at $|Q| \sim 3.28$. Because $\mu_{\rm ex} \to 0$ as $|Q| \to 0$, there also exists a tensor-unstable mass range in neutral cases.

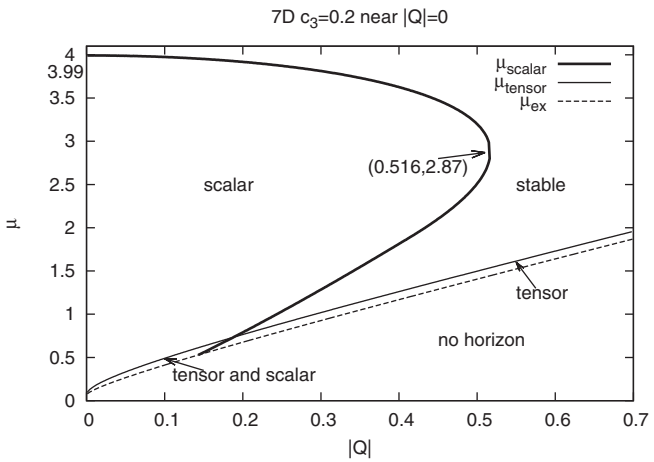

Fig. 6. Numerical results for 7 dimensions. We calculate these with $c_3 = 0.2$. Both $\mu_{\rm tensor}$ and $\mu_{\rm ex}$ converge to 0.667 as $Q \to 0$. Thus there is no instability under tensor perturbations in the neutral case. Note that there exists no ghost region in $c_2 = 0.2$. The appearances of the diagrams do not strongly depend on c_3 except for the ghost regions.

$\mu \sim 3.99$ and this region vanishes at $|Q| \sim 0.516$. When c_3 changes, the upper bound etc. change but the appearances of these unstable regions do not change.

When $c_3 = 0.2$, there is no ghost region. However, when c_3 is larger than 0.25, we can find a ghost region near the origin of the diagram (see Fig. 14 in our previous paper [34]).

Therefore, like 5 dimensions, we can roughly say that the black hole suffers from instability under scalar perturbations if $Q \sim 0$ and μ is smaller than a certain value and shows instability under tensor modes when μ is as small as $\mu_{\rm ex}$. In contrast with the 5-dimensional case, there exists c_3-dependence for the ghost region.

6.4. *8 dimensions*

We present the two figures for 8 dimensions. Figure 7 shows the numerical result for $c_3 = 0.07$; we calculate the region in $\mu_{\rm ex}(|Q|) < \mu < \mu_{\rm ex}(|Q|) + 0.05$ and the mesh size is $d\mu = dQ = 10^{-4}$. This figure is almost the same as that for 6-dimensional case. In this figure, there is no parameter that makes $2T'^2 - TT''$ negative, so we can only find instability under tensor-type perturbations. For tensor-type perturbations, the unstable region lies slightly on $\mu_{\rm ex}(|Q|)$ and there also exists a gap between $\mu_{\rm tensor}$ and $\mu_{\rm ex}$ in $|Q| \to 0$. These properties are similar to the 6-dimensional case.

In contrast with the above results, there exists a scalar-unstable region in Fig. 8. This figure is calculated with $c_3 = 1$ and checks the region in $\mu_{\rm ex}(|Q|) < \mu < \mu_{\rm ex}(|Q|) + 30$ with the mesh size $d\mu = dQ = 10^{-3}$. This figure is very similar to the 5-dimensional diagram; a tensor-unstable region exists just on the extreme line $\mu_{\rm ex}(|Q|)$ and a scalar-unstable region localizes near the μ-axis. Furthermore, there is no ghost region in $c_3 = 1$.

In Figs. 7 and 8, there is no ghost region. However, when c_3 becomes larger than 5.92, a ghost region appears near the origin of the diagram (see Fig. 18 in Ref. [34]). Thus, the appearance is similar to the 7-dimensional case with sufficiently large c_3.

In 8 dimensions, as we have shown, the diagram's appearance is very sensitive to the Lovelock coupling c_3. When c_3 is very small, this is the same as the 6-dimensional diagram. As c_3 becomes

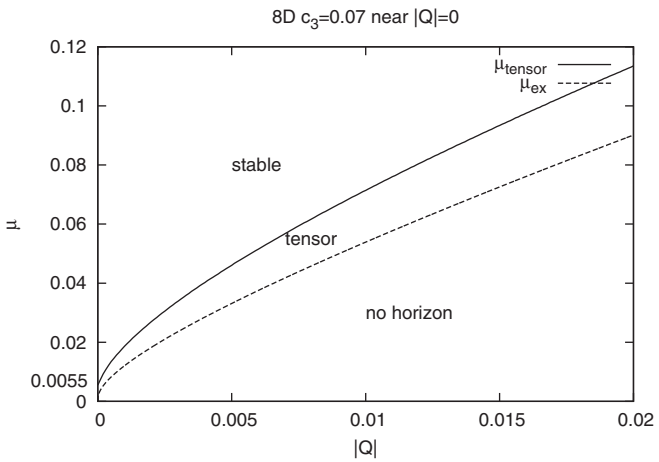

Fig. 7. Numerical results for 8 dimensions with $c_3 = 0.07$. The appearance of this figure is very similar to the result for 6 dimensions; there only exists a tensor-unstable region near the extreme line $\mu_{\rm ex}(|Q|)$. $\mu_{\rm tensor}$ converges to 0.0055 and $\mu_{\rm ex}$ tends to 0 when $|Q| \to 0$. Thus there also exists instability under tensor-type perturbations when black holes are neutral. We cannot find ghost regions and scalar-unstable regions in $c_3 = 0.07$.

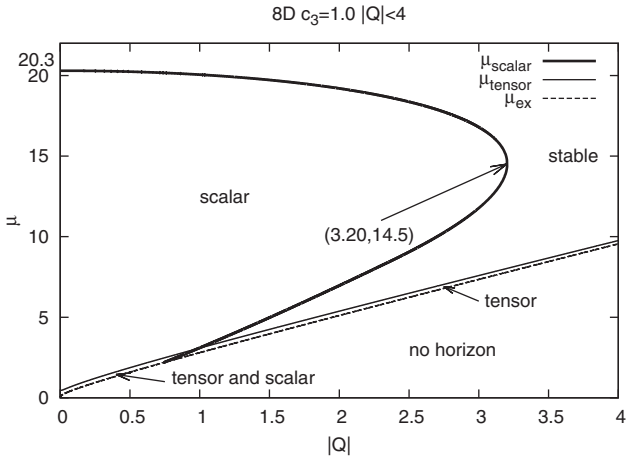

Fig. 8. Numerical results for 8 dimensions with $c_3 = 1$. In contrast with the $c_3 = 0.07$ case, there exists a scalar-unstable region near $|Q| = 0$. Thus, in 8 dimensions, the type of instability that black holes suffer from is very sensitive to third-order Lovelock coupling c_3. In this figure, $\mu_{\rm ex} \to 0$ and $\mu_{\rm tensor} \to 0.459$ as $|Q| \to 0$. Note that we cannot find ghost regions in $c_3 = 1$.

larger, the appearance of the diagram changes from the 5-dimensional result to the 7-dimensional diagram with large c_3. It is still an open issue why such dramatic changes occur in 8 dimensions.

6.5. Summary of numerical results

In this section, we have numerically checked the conditions for the instability and the ghost. Here, we summarize the results.

We numerically examine the behavior of $T(r)$ for various Lovelock couplings in 5, 6, 7, and 8 dimensions and plot the results in Q–μ diagrams. From these results, we can read some common properties. The first is the locations of unstable regions. The unstable regions for tensor-type perturbations lie slightly on the extreme line $\mu_{\rm ex}$. The regions for scalar-type perturbations, if they exist, localize at the μ-axis and extend to relatively large μ. The second is the behavior of tensor-unstable region near $|Q| = 0$ when there is no scalar-unstable region. For this case, in our numerical calculation, there must exist a slight mass range in which black holes show instability under tensor perturbations. Therefore, whether a scalar-unstable region exists or not, when black holes with nearly extreme mass have a slight charge, they must be unstable; the type of instability they have depends on their parameters and dimensions, but they have at least one type of instability.

These results also lead to some open questions. The first is the dimensionality. The diagrams for the 5-dimensional and 7-dimensional cases are very similar: the results for 6 dimensions and 8 dimensions with small c_3 are alike. These remind us that the behaviors of black holes against perturbations are different in even and odd dimensions. However, we do not have the answer to such dimension-dependences. The second question is the response to variations of the Lovelock couplings. For example, in 8 dimensions, the appearance of the diagram is sensitive to the third-order coupling c_3. These are still open questions as to whether this is proper to 8 dimensions or not and what causes such peculiarities.

7. Conclusion

We have studied the stability of charged Lovelock black hole solutions. We have derived master equations for vector-type perturbations and scalar-type perturbations. These are Schrödinger equations

with two components. For vector-type perturbations, we have shown that the Schrödinger operator for this type of perturbation is an essentially self-adjoint positive-definite operator. Thus charged Lovelock black holes are stable under vector-type perturbations. For scalar-type perturbations, we have presented the condition for instability. In detail, if $2T'^2 - TT''$ has negative regions, charged Lovelock black holes are unstable under scalar-type perturbations. For tensor-type perturbations, we have already shown that T' and T'' are crucial for the stability. By checking these criteria numerically, e.g. in the second- and third-order Lovelock theory, we have shown that there exist unstable parameters; nearly extreme black holes show instability under tensor-type perturbations, and black holes with small charge show instability under scalar-type perturbations even if the black holes have relatively large mass.

One piece of work for the future is the exploration of more general conditions for stability under scalar-type perturbations. In this paper, we have shown that black holes are unstable if $2T'^2 - TT''$ has negative regions. However, the inverse statement has not been proved. Hence, so far, we cannot say anything when $2T'^2 - TT''$ is always positive. Furthermore, by this criterion, we cannot detect instability under scalar-type perturbations in Einstein theory [12]. In this sense, it would be interesting to discover more general conditions.

It would be interesting to investigate the relation between the dynamical instability we have shown in this paper and thermodynamics. On the thermodynamics for Lovelock black holes, variations of the Lovelock coefficients are also examined in Ref. [37]. In our paper, we have found that the appearance of the $Q - \mu$ diagrams changes dramatically as the Lovelock coupling c_3 varies in 8 dimensions. Thus it would be interesting to see if such dramatic changes were found in the thermodynamics.

The relationship between instabilities and gravitational collapses might be important. In Lovelock theory, collapses of dusts have been examined [38,39]. Furthermore, these have been extended to charged dust clouds [40]. In these, the dependence of the dimensions is found for, e.g., naked singularity formations. Our results also depend on the dimensions, so there may exist relationships between instability and gravitational collapse in Lovelock gravity. In dust collapses, the authors of the above papers have also pointed out the tendency that the higher curvature collections suppress formations of apparent horizons. These results should show that the higher curvature collections make the attractive force weaker, and this property might be related to the instability of Lovelock black holes that we have discussed in this paper.

Acknowledgement

The author would like to thank Akihiro Ishibashi, Jiro Soda, and Seiju Ohashi for useful comments and fruitful discussions. This work is supported by the Japan Society for the Promotion of Science (JSPS) grant No. 23–661 and a Grant-in-Aid for the Global COE Program "The Next Generation of Physics, Spun from Universality and Emergence" from the Ministry of Education, Culture, Sports, Science and Technology (MEXT) of Japan.

References

[1] S. B. Giddings and S. D. Thomas, Phys. Rev. D **65**, 056010 (2002).
[2] S. B. Giddings and M. L. Mangano, Phys. Rev. D **78**, 035009 (2008).
[3] F. R. Tangherlini, Nuovo Cimento **27**, 636 (1963).
[4] R. C. Myers and M. J. Perry, Ann. Phys. **172**, 304 (1986).
[5] R. Emparan and H. S. Reall, Phys. Rev. D **65**, 084025 (2002).
[6] H. Iguchi and T. Mishima, Phys. Rev. D **75**, 064018 (2007); **78**, 069903 (2008) [erratum].
[7] H. Elvang and P. Figueras, J. High Energy Phys. **0705**, 050 (2007).
[8] H. Kodama and A. Ishibashi, Prog. Theor. Phys. **110**, 701 (2003).
[9] A. Ishibashi and H. Kodama, Prog. Theor. Phys. **110**, 901 (2003).

[10] A. Ishibashi and H. Kodama, Prog. Theor. Phys. Suppl. **189**, 165 (2011).
[11] H. Kodama and A. Ishibashi, Prog. Theor. Phys. **111**, 29 (2004).
[12] R. A. Konoplya and A. Zhidenko, Nucl. Phys. B **777**, 182 (2007).
[13] O. J. C. Dias, P. Figueras, R. Monteiro, J. E. Santos, and R. Emparan, Phys. Rev. D **80**, 111701 (2009).
[14] O. J. C. Dias, P. Figueras, R. Monteiro, and J. E. Santos, Phys. Rev. D **82**, 104025 (2010).
[15] K. Murata, Prog. Theor. Phys. Suppl. **189**, 210 (2011).
[16] N. Tanahashi and K. Murata, arXiv:1208.0981 [hep-th].
[17] P. Figueras, K. Murata, and H. S. Reall, Classical Quantum Gravity **28**, 225030 (2011).
[18] D. Lovelock, J. Math. Phys. **13**, 874 (1972).
[19] D. Lovelock, J. Math. Phys. **12**, 498 (1971).
[20] D. G. Boulware and S. Deser, Phys. Rev. Lett. **55**, 2656 (1985).
[21] D. G. Boulware and S. Deser, Phys. Lett. B **175**, 409 (1986).
[22] R. Zegers, J. Math. Phys. **46**, 072502 (2005).
[23] C. Charmousis, *Lecture Notes in Physics* (Springer, Heidelberg, 2009) Vol. 769, p. 299.
[24] C. Garraffo and G. Giribet, Mod. Phys. Lett. A **23**, 1801 (2008).
[25] H. Maeda, S. Willison, and S. Ray, Classical Quantum Gravity **28**, 165005 (2011).
[26] J. T. Wheeler, Nucl. Phys. B **273**, 732 (1986).
[27] G. Dotti and R. J. Gleiser, Classical Quantum Gravity **22**, L1 (2005).
[28] G. Dotti and R. J. Gleiser, Phys. Rev. D **72**, 044018 (2005).
[29] R. J. Gleiser and G. Dotti, Phys. Rev. D **72**, 124002 (2005).
[30] M. Beroiz, G. Dotti, and R. J. Gleiser, Phys. Rev. D **76**, 024012 (2007).
[31] R. A. Konoplya and A. Zhidenko, Phys. Rev. D **77**, 104004 (2008).
[32] T. Takahashi and J. Soda, Prog. Theor. Phys. **124**, 911 (2010).
[33] T. Takahashi and J. Soda, Prog. Theor. Phys. **124**, 711 (2010).
[34] T. Takahashi, Prog. Theor. Phys. **125**, 1289 (2011).
[35] R. C. Myers and J. Z. Simon, Phys. Rev. D **38**, 2434 (1988).
[36] G. Kofinas and R. Olea, J. High Energy Phys. **0711**, 069 (2007).
[37] D. Kastor, S. Ray, and J. Traschen, Classical Quantum Gravity **27**, 235014 (2010).
[38] H. Maeda, Class. Quantum Grav. **23**, 2155 (2006).
[39] S. Ohashi, T. Shiromizu, and S. Jhingan, Phys. Rev. D **84**, 024021 (2011).
[40] S. Ohashi, T. Shiromizu, and S. Jhingan, Phys. Rev. D **86**, 044008 (2012).